Applications of Subsurface Microscopy

Laurene Tetard[1,2], Ali Passian[1,2*], Rubye H. Farahi[1,2], Brynn H. Voy[1,3], Thomas Thundat[1,2]

[1] Oak Ridge National Laboratory, Oak Ridge, TN 37831-6123, USA

[2] Department of Physics, University of Tennessee, Knoxville, TN 37996, USA

[3] Department of Animal Science, University of Tennessee, Knoxville, TN 37996, USA

***Corresponding author:** passianan@ornl.gov

Running Head: Subsurface Microscopy

Summary

Exploring the interior of a cell is of tremendous importance in order to assess the effects of nanomaterials on biological systems. Outside of a controlled laboratory environment, nanomaterials will most likely not be conveniently labeled or tagged so that their translocation within a biological system cannot be easily identified and quantified. Ideally, the characterization of nanomaterials within a cell requires a nondestructive, label-free, and subsurface approach. Subsurface nanoscale imaging represents a real challenge for instrumentation. Indeed the tools available for high resolution characterization, including optical, electron or scanning probe microscopies, mainly provide topography images or require tagants that fluoresce. Although the intercellular environment holds a great deal of information, subsurface visualization remains a poorly explored area. Recently, it was discovered that by mechanically perturbing a sample, it was possible to observe its response in time with nanoscale resolution by probing the surface with a micro-resonator such as a microcantilever probe (Figure 1). Microcantilevers are used as the force-sensing probes in Atomic Force Microscopy (AFM), where the nanometer-scale probe tip on the microcantilever interacts with the sample in a highly controlled manner to produce high-resolution raster-scanned information of the sample surface. Taking advantage of the existing capabilities of AFM, we present a novel technique, Mode Synthesizing Atomic Force Microscopy (MSAFM) (Figure 1), which

has the ability to probe subsurface structures such as non-labeled nanoparticles embedded in a cell. In MSAFM mechanical actuators (PZTs) excite the probe and the sample at different frequencies as depicted in Figure 1. The nonlinear nature of the tip-sample interaction, at the point of contact of the probe and the surface of the sample, in the contact mode AFM configuration permits the mixing of the elastic waves. The new dynamic system comprises new synthesized imaging modes, resulting from sum- and difference-frequency generation of the driving frequencies. The specific electronics of MSAFM allows the selection of individual modes and the monitoring of their amplitude and phase. From these quantities of various synthesized modes a series of images can be acquired. The new images contain subsurface information, thus revealing the presence of nanoparticles inside the cells.

Key Words

Nanotoxicology, Microscopy, Subsurface, Ultrasonic Microscopy, Atomic Force Microscopy, Mode Synthesizing Atomic Force Microscopy, Nanoparticles

1. Introduction

An increasing array of engineered nanomaterials is under development for diverse industrial, consumer and medical applications **(*1-4*).** In parallel, safety and health issues related to nanoparticles exposure continue to be debated **(*5-10*)**. The new area of research to address potential safety concerns consists of toxicity studies, development of novel methods, screenings and characterization of nanomaterials and their effect on biological systems is now referred to as nanotoxicology **(*10-13*)**. Assessing potential toxicity is complicated by a number of factors **(*14*)**. One of the most significant challenges is the ability to track the fate of nanomaterials as they enter the body and potentially penetrate biological tissue, which requires the ability to noninvasively monitor the response of the system with high spatial resolution. Furthermore, a number of studies **(*6, 9, 14, 15*)** suggest that particle-specific toxicity studies are necessary, with a careful screening for key characteristics such as the size **(*12*)**, the shape, the

crystallinity, the chemical composition, the surface properties (area, chemistry or charge) (***16***), to reach a full understanding of the mechanisms of the nanoparticle-biomaterial interaction. Imaging techniques capable of localizing and visualizing nanoparticles with nanometer resolution while keeping the cellular structure intact are therefore of tremendous importance (***2***). The development of analytical techniques to assess biodistribution, translocation and cellular uptake, both *in vivo* and *in vitro*, is a key component for the advancement of the field. The ability to track nanoparticles uptake at the level of a single cell would allow mechanistic studies of particle translocation and distribution within a cell, which are central to dissecting potential biological effects. Further, with respect to screening for exposures, such a technique would create a tool to examine a surrogate biological sample such as peripheral blood that could be collected with minimal invasion. We focus here on the visualization of nanoparticles inside animal cells using a novel technique called Mode Synthesizing Atomic Force Microscopy (MSAFM)(***17-20***). We also review the various technologies, which have been used to determine the presence of nanoparticles in cells.

Optical imaging

Confocal microscopy is a powerful optical imaging technique commonly used in biology. Confocal imaging has the ability to noninvasively investigate an organism and reconstruct a 3D image of the system, providing insights on the structure and behavior of the system, an important attribute for nanotoxicology studies. Many studies have reported the subcellular localization of nanoparticles in cells using confocal fluorescence microscopy (***15, 21, 22***). Fluorescence measurements are carried out by labeling the nanoparticles before permitting them to interact with the cell cultures. Although this process allows recognition and tracking of the nanoparticles in the different organelles of the cell, the dyes used as labels make it difficult to separate the biological properties of the nanoparticles from the action of the dyes. With techniques such as confocal microscopy, bright field or dark field microscopy, it is only possible to observe phenomena (delivery, cellular uptake, etc.) of nanomaterials larger than the diffraction limit of light. It is then necessary to turn to other complementary techniques for advanced studies involving lower concentration of nanoparticles and their localized interaction with biological tissues (***21***).

Electron microscopy

Electron microscopy is an imaging technique commonly used in nanotoxicology studies, owing to its high spatial resolution and depth of field **(*23, 24*)** capability. Scanning electron microscopy (SEM) and transmission electron microscopy (TEM) provide important insight in nanomaterial characterization. SEM is usually used for morphology inspection of the cells before and after exposure to the nanoparticles. Attempts to use TEM to locate nanotubes within alveolar macrophages positively identify only aggregates **(*24, 25*)**. Porter et al. reported the observation of carbon nanotubes in lysosomes **(*25*)**. However, the composition of cells is rich in carbon. One of the difficulties encountered when using electron microscopy to trace nanoparticles inside a cell is the low contrast between the cell structures and the nanomaterials, in particular for unlabelled carbon-based particles such as carbon nanotubes **(*25*)**. Staining the sample sections prior to performing TEM imaging can be performed in order to increase the contrast between nanomaterials and cell structures. However, it is time consuming, labor-intensive, and requires the use of heavy metal (osmium tetroxide, uranyl acetate, lead citrate) that may disrupt the biological sample. Other electron microscope-based approaches, such as electron energy loss (EEL) or energy-dispersive x-ray spectroscopies have also been used to trace nanoparticle uptake in cells **(*25*)**. The information extracted from the bulk Plasmon peak in the EEL **(*26*)** data revealed the presence of carbon nanotubes in the lysosomes of the cell after 2 days.

Confocal fluorescent and electron microscopy are best used together to get a good representation of material uptake and localization. However, in many cases, for instance when unlabelled carbon nanoparticles are involved, it remains difficult to locate and identify single nanoparticles within a cell. It is even more complex and challenging to operate on living cells, especially in the high-vacuum conditions of electron microscopy.

Scanning Probe Microscopy

A range of techniques in scanning probe microscopy (SPM) are available to noninvasively characterize materials, and access physical, structural and chemical properties with high spatial resolution **(*27*)**. Atomic force microscopy (AFM) is now widely used in life sciences **(*28-30*)**. It is advantageous because of simpler sample preparation and the ability for ambient imaging. However, conventional AFM typically

only probes the surface of a specimen, making it difficult to analyze structures within a cell **(*31*).** AFM imaging is generally performed using contact or tapping mode imaging. In contact mode, the tip of the cantilever probe is in direct contact with the sample during the image scan, exerting a force of 50-100pN on the sample at all times. In tapping mode, the cantilever is mechanically excited close to its resonance frequency. The tip and the sample contact only at the lowest position of the oscillation, significantly decreasing the forces applied on the sample. Tapping mode is very popular in biological applications **(*28, 29*)**, especially for imaging of soft samples or samples that are not well attached to the substrate, which is generally the case in liquid environments. The measurements performed in contact or tapping provide insight on the surface and interfacial properties on the system of interest. However, subsurface imaging with nanoscale resolution has remained an unexplored area **(*32-35*)**. One may envision this limitation as being due to a lack of mechanical excitation of the sample resulting in the inability of the probe to gather the subsurface dynamic attributes **(*36-39*)**. MSAFM **(*19, 20*)** offers a potential circumvention that is capable of subsurface imaging of soft samples and thus is a potential method for probing cellular uptake of nanoparticles. The phase information in the coupled modes may be detected at various frequencies corresponding to a synthesized mode **(*20*),** which can be displayed as a function of the spatial location of the scanning cantilever tip (Figure 1). The resultant amplitude or phase map may then reveal any contrasts due to acoustic impedance variation that results from nanoscale heterogeneity in a volume of the cell directly underneath the AFM tip and amounts to a mapping of the cell's elastic response. We explored this viability by using MSAFM to determine the cellular fate of Single-Wall Carbon Nanohorns (SWCNH) and silica nanospheres using a mouse model to detect and visualize particles within lavage macrophages and erythrocytes (blood cells) **(*18, 19*)** as described in Figure 2.

2. Materials

Sample preparation

1. Isoflurane anesthesia, to sacrifice the mice

2. Bell jar or other air-tight container for anesthesia
3. Blunt 22-gauge needle for bronchoalveolar lavage (BAL) fluid collection
4. Cold sterile Phosphate Buffered Saline (PBS)
5. Sterile tubes (1.5 ml)
6. Cytospin
7. Hematology stain (e.g., Hema3, Fisher Scientific)
8. Cleaved mica (see Note 1)
9. Methanol
10. Heparinized capillary tubes for blood collection
11. Mica substrates for the samples

3. Methods

A. Sample

In order to study the fate of the nanoparticles in biological system, it is important to choose a route of exposure corresponding to a real life situation. For instance, pharyngeal aspiration has been reported as an efficient method for exposure and distribution of nanoparticles throughout the alveolar regions of the lungs. In the case of carbon nanoparticles, the OSHA-permissible limit of exposure across twenty eight-hours days is equivalent to exposing a mouse to 30 μg of carbon nanohorns SWCNH. The nanoparticles were administered by pharyngeal aspiration after anaesthetizing the mice with isoflurane. The solution of nanoparticles or the control solutions were applied in a bolus on the back of the tongue, which is extended using forceps. The tongue was released after the fluid is fully aspired into the lungs. The mouse was allowed to recover in his home cage after exposure and anesthetized at time points of choice for collection of BAL fluid and/or blood, as follows:

1. Mice are sacrificed by isoflurane overdose in a bell jar

2. Bronchoalveolar lavage (BAL) fluid is collected according to standard protocols (reference Rachel's paper)
3. The trachea is exposed and a blunt 22-gauge needle inserted into the trachea. After securing the needle with sutures, lavage is performed five times with cold sterile PBS.
4. Fluid is gently aspirated while massaging the chest. The first lavage is performed with 0.6ml of PBS and was kept separate for analysis for another study.
5. The second and third lavages are performed with 1.0ml of PBS and are pooled in sterile tubes, centrifuged, and resuspended in PBS.
6. For light microscopy analysis, cytospin slides are stained with a Hema3 kit.
7. For AFM analysis, cells are centrifuged onto freshly cleaved mica (see Note 1) using a cytospin and fixed with methanol (see Note 2 and 3).
8. Peripheral blood is collected from the abdominal aorta into heparinized capillary tubes.
9. Blood samples are diluted in PBS, centrifuged onto freshly cleaved mica using a cytospin, and fixed with methanol (see Note 2 and 3).
10. The mica substrate is affixed onto the sample actuator with glue.

B. Mode Synthesizing Atomic Force Microscopy

The MSAFM was developed on a modified multimode AFM (Nanoscope III, Digital Instrument). MSAFM operates on the basis of expanding the dynamic attributes of the probe and the sample of an AFM to boost the frequency content of the system. Actuators, located at the base of the cantilever and the sample (Figure 1), exerted mechanical forces on the probe and the substrate, respectively (see Note 4 and 5), of the order of few kilohertz to several tens of megahertz. The acoustic waves, created at the bottom of the sample, transmitted through the sample and modified the position of the tip of the cantilever that is in contact with the sample (see Note 6). At the tip-sample interface, the nanomechanical interaction resulted in a nonlinear force that leads to difference and sum frequency generation yielding a series of synthesized oscillations via higher order coupling in the system. The evolution of the probe's state in time is

monitored using the position sensitive detector of the AFM. The resulting signal S(t) is interpreted as a contrast map, representative of the forces at each point of the scanned area. In Fourier space, S(t) takes the form of a rich spectrum, in which the synthesized modes created in the system are engaged for amplitude or phase imaging. An MSAFM session can be established from the following instructions:

1. The laser of the optical read-out system is aligned with the cantilever.
2. The sample is mounted on the AFM sample holder.
3. Using the MSAFM module, the actuators are connected to waveform generators.
4. The approach is executed by engaging the cantilever for contact imaging (see Note 2).
5. The excitation frequencies are tuned to generate a set of frequencies interesting to probe the sample.
6. The frequencies of the modes of interest are selected. These frequencies will be used as reference in the lockin measurement stage.
7. The signal input S(t) is sent as inputs for lockin measurements. The resulting signals (amplitudes or phases) are recorded.
8. The mode of images to be displayed (mode, amplitude, or phase) is selected. A standard AFM topography image is obtained along with amplitude and phase images extracted from the MSAFM module.

The resulting images, presented in Figure 3, display the surface and subsurface information of the sample, including embedded particles (see Note 7). The morphology of the nanoparticles alone was examined using standard AFM imaging. Similar measurements, presented in Figure 4, were carried out for silica nanopsheres **(*17, 18*)**. Silica and carbon have very different elastic properties (stiffness and density).

C. Spectroscopy measurements

Although the MSAFM images reveal the presence of nanoscale features inside the cell, their chemical composition remains unknown. The portfolio of tools capable of imaging cell structures with high

resolution is very limited for chemical recognition. For example, spectroscopic measurements are diffraction limited.

We carried out Raman spectroscopy measurements on the samples in order to corroborate the presence/absence of carbon nanohorns inside the cell **(*19*)** (see Note 8). The results are presented in Figure 5. The Raman spectra were obtained from a Renishaw micro-Raman spectrometer, equipped with a 785nm Near Infrared laser and a Leica Raman Imaging microscope. In micro-Raman spectroscopy, the Near IR laser is used in conjunction with an optical microscope to excite the sample, and the inelastic scattering resulting from the light impinging the sample is monitored using a monochromator and photon sensitive detector. Raman effect results from the relaxation of the excited molecules accompanied by the photon emission while the molecules return to a lower energy state. The following steps can be followed to carry out the Raman measurements:

1. Prepare the sample of a substrate that is transparent to the excitation light source; here we used glass.
2. Perform a background scan to ensure that the focus of the microscope is optimized.
3. Insert the sample in the beam path in the sample compartment.
4. Perform control measurements on the as-produced nanomaterial.
5. Perform the measurements on the cell samples. Depending on the model of the microspectrometer, it is possible to obtain spectra at various locations of the sample by manual translation or taking advantage of an automated X-Y stage.

This procedure is important in order to identify the regions where nanoparticles are present. One of the major drawbacks is the lack of spatial resolution and sensitivity for lower concentration of nanomaterials. However, the observations made with MSAFM were strengthened by the Raman spectroscopy measurements, confirming the presence of carbon nanohorns in the macrophages **(*17, 19*)**.

4. Notes

1. The surfaces usually used for AFM sample preparation include silicon (wafer), mica, glass (slide), or gold surfaces. Special precautions should be taken to ensure the surface properties of the substrate (hydrophobic/hydrophilic, electrostatic…) and those of the sample are compatible. Mica substrates should be used because the glass slides readily respond to ultrasonic waves.
2. The measurements were carried out on dried samples in ambient conditions. At the scale of the tip, there exists a thin water film at the surface of the sample. Because of the capillary forces created by the meniscus between the tip and the sample, the resolution is not optimum when operated in contact mode. Imaging in liquid, although minimizing capillary and hydrophobic/hydrophilic forces, would also present new challenges due to the new liquid environment **(*28, 29*)**.
3. Imaging in liquid should be considered for better preservation of the cell structure and minimization of capillary and hydrophobic/hydrophilic forces.
4. In the case of our study the actuators that created the mechanical stimulus to the probe and sample were piezoelectric crystals.
5. Improvements can be made in the contact between sample and sample actuator.
6. The microcantilever properties, such as spring constant, length and probe tip shape, determine the quality of the images. Softer cantilevers (i.e. less stiff) should be used to preserve the cells. One should have a precise idea of the conditions of operation for a given measurements, such as the forcing amplitude and frequencies, in order to assess the best suited microcantilever probe.
7. Salt can crystallize and create crystals on the sample, making it difficult to locate engineered embedded nanoparticles. Contamination is a serious problem in the preparation of samples for AFM studies, since AFM resolves nanometer scale features.
8. There is a need for some kind of chemical characterization to ensure that the features revealed by the images are the nanoparticles. One of the major drawbacks remains the lack of sensitive and specific high spatial resolution chemical identification techniques.

5. References

1. Fan, X., Tan, J., Zhang, G., and Zhang, F. (2007) Isolation of carbon nanohorn assemblies and their potential for intracellular delivery, *Nanotechnology 18*.
2. Stone, V., and Donaldson, K. (2006) Nanotoxicology - Signs of stress, *Nature Nanotechnology 1*, 23-24.
3. Sadik, O. A., Zhou, A. L., Kikandi, S., Du, N., Wang, Q., and Varner, K. (2009) Sensors as tools for quantitation, nanotoxicity and nanomonitoring assessment of engineered nanomaterials, *Journal of Environmental Monitoring 11*, 1782-1800.
4. Strassert, C. A., Otter, M., Albuquerque, R. Q., Hone, A., Vida, Y., Maier, B., and De Cola, L. (2009) Photoactive Hybrid Nanomaterial for Targeting, Labeling, and Killing Antibiotic-Resistant Bacteria, *Angewandte Chemie-International Edition 48*, 7928-7931.
5. Colvin, V. (2003) The potential environmental impact of engineered nanomaterials, *Nature Biotechnology 21*, 1166-1170.
6. Holsapple, M., Farland, W., Landry, T., Monteiro-Riviere, N., Carter, J., Walker, N., and Thomas, K. (2005) Research strategies for safety evaluation of nanomaterials, part II: Toxicological and safety evaluation of nanomaterials, current challenges and data needs, *Toxicological Sciences 88*, 12-17.
7. Kreyling, W. G., Semmler-Behnke, M., and Moeller, W. (2006) Health implications of nanoparticles, *Journal of Nanoparticle Research 8*, 543-562.
8. Medina, C., Santos-Martinez, M. J., Radomski, A., Corrigan, O. I., and Radomski, M. W. (2007) Nanoparticles: pharmacological and toxicological significance, *British Journal of Pharmacology 150*, 552-558.
9. Nel, A., Xia, T., Madler, L., and Li, N. (2006) Toxic potential of materials at the nanolevel, *Science 311*, 622-627.
10. Oberdorster, G., Oberdorster, E., and Oberdorster, J. (2005) Nanotoxicology: An emerging discipline evolving from studies of ultrafine particles, *Environmental Health Perspectives 113*, 823-839.
11. Myllynen, P. (2009) Nanotoxicology: Damaging DNA from a distance, *Nat Nano 4*, 795-796.
12. Dawson, K. A., Salvati, A., and Lynch, I. (2009) Nanotoxicology: Nanoparticles reconstruct lipids, *Nat Nano 4*, 84-85.
13. Donaldson, K., and Poland, C. A. (2009) Nanotoxicology: New insights into nanotubes, *Nat Nano 4*, 708-710.
14. Donaldson, K., Aitken, R., Tran, L., Stone, V., Duffin, R., Forrest, G., and Alexander, A. (2006) Carbon nanotubes: A review of their properties in relation to pulmonary toxicology and workplace safety, *Toxicological Sciences 92*, 5-22.
15. Verma, A., Uzun, O., Hu, Y., Hu, Y., Han, H.-S., Watson, N., Chen, S., Irvine, D. J., and Stellacci, F. (2008) Surface-structure-regulated cell-membrane penetration by monolayer-protected nanoparticles, *Nat Mater 7*, 588-595.
16. Auffan, M., Rose, J., Bottero, J.-Y., Lowry, G. V., Jolivet, J.-P., and Wiesner, M. R. (2009) Towards a definition of inorganic nanoparticles from an environmental, health and safety perspective, *Nat Nano 4*, 634-641.

17. Tetard, L., Passian, A., Farahi, R. H., and Thundat, T. (2010) Atomic force microscopy of silica nanoparticles and carbon nanohorns in macrophages and red blood cells, *Ultramicroscopy 6*, 586-591.
18. Tetard, L., Passian, A., Lynch, R. M., Voy, B. H., Shekhawat, G., Dravid, V. P., and Thundat, T. (2008) Elastic phase response of silica nanoparticles buried in soft matter, *Applied Physics Letters 93*, 133113.
19. Tetard, L., Passian, A., Venmar, K. T., Lynch, R. M., Voy, B. H., Shekhawat, G., Dravid, V. P., and Thundat, T. (2008) Imaging nanoparticles in cells by nanomechanical holography, *Nature Nanotechnology 3*, 501-505.
20. Tetard, L., Passian, A., and Thundat, T. (2010) New modes for subsurface atomic force microscopy through nanomechanical coupling, *Nature Nanotechnology 5*, 105-109.
21. Panyam, J., Sahoo, S. K., Prabha, S., Bargar, T., and Labhasetwar, V. (2003) Fluorescence and electron microscopy probes for cellular and tissue uptake of poly(,-lactide-co-glycolide) nanoparticles, *International Journal of Pharmaceutics 262*, 1-11.
22. Zhang, Y., Kohler, N., and Zhang, M. (2002) Surface modification of superparamagnetic magnetite nanoparticles and their intracellular uptake, *Biomaterials 23*, 1553-1561.
23. Geiser, M., Rothen-Rutishauser, B., Kapp, N., Schurch, S., Kreyling, W., Schulz, H., Semmler, M., Hof, V., Heyder, J., and Gehr, P. (2005) Ultrafine particles cross cellular membranes by nonphagocytic mechanisms in lungs and in cultured cells, *Environmental Health Perspectives 113*, 1555-1560.
24. Worle-Knirsch, J., Pulskamp, K., and Krug, H. (2006) Oops they did it again! Carbon nanotubes hoax scientists in viability assays, *Nano Letters 6*, 1261-1268.
25. Porter, A. E., Gass, M., Muller, K., Skepper, J. N., Midgley, P. A., and Welland, M. (2007) Direct imaging of single-walled carbon nanotubes in cells, *Nature Nanotechnology 2*, 713-717.
26. Daniels, H. R., Brydson, R., Brown, A., and Rand, B. (2003) Quantitative valence plasmon mapping in the TEM: viewing physical properties at the nanoscale, *Ultramicroscopy 96*, 547-558.
27. Lang, H. P., and Gerber, C. (2009) Up close & personal with atoms & molecules, *Materials Today 12*, 18-25.
28. Allison, D. P., Mortensen, N. P., Sullivan, C. J., and Doktycz, M. J. (2010) Atomic force microscopy of biological samples, *Wiley Interdisciplinary Reviews-Nanomedicine and Nanobiotechnology 2*, 618-634.
29. Kim, S., Kihm, K. D., and Thundat, T. (2010) Fluidic applications for atomic force microscopy (AFM) with microcantilever sensors, *Experiments in Fluids 48*, 721-736.
30. Mao, Y. D., Sun, Q. M., Wang, X. F., Ouyang, Q., Han, L., Jiang, L., and Han, D. (2009) In vivo nanomechanical imaging of blood-vessel tissues directly in living mammals using atomic force microscopy, *Applied Physics Letters 95*.
31. Garcia, R., Margerle, R., and Perez, R. (2007) Nanoscale compositional mapping with gentle forces, *Nature Mater. 6*, 405-411.
32. Chung, J., Kim, K., Hwang, G., Kwon, O., Lee, J. S., Park, S. H., and Choi, Y. K. (2010) Nanoscale range finding of subsurface structures by measuring the absolute phase lag of thermal wave, *Review of Scientific Instruments 81*.
33. Shekhawat, G., Srivastava, A., Avasthy, S., and Dravid, V. (2009) Ultrasound holography for noninvasive imaging of buried defects and interfaces for advanced interconnect architectures, *Applied Physics Letters 95*.

34. Shekhawat, G. S., Avasthy, S., Srivastava, A. K., Tark, S. H., and Dravid, V. P. (2010) Probing Buried Defects in Extreme Ultraviolet Multilayer Blanks Using Ultrasound Holography, *Ieee Transactions on Nanotechnology 9*, 671-674.
35. Valdes, O., and Cuberes, M. T. (2009) Characterization of a New Scaffold Formed of Polyelectrolyte Complexes Using Atomic Force and Ultrasonic Force Microscopy, *Journal of Biomedical Nanotechnology 5*, 716-721.
36. Rabe, U., and Arnold, W. (1994) Acoustic microscopy by atomic force microscopy, *Applied Physics Letters 64*, 1493-1495.
37. Kolosov, O. V., Martin, R. C., Marsh, C. D., Briggs, G. A., Kamins, T. I., and Williams, R. S. (1998) Imaging the Elastic Nanostructures of Ge Islands by Ultrasonic Force Microscopy, *Physical Review Letters 81*, 1046.
38. Martinez, N. F., Patil, S., Lozano, J. R., and Garcia, R. (2006) Enhanced compositional sensitivity in atomic force microscopy by the excitation of the first two flexural modes, *Applied Physics Letters 89*.
39. Sahin, O. (2008) Scanning below the cell surface, *Nature Nanotechnology 3*, 461-462.

Acknowledgements:

The study was supported by the Oak Ridge National Laboratory (ORNL) Technology Maturation Fund. ORNL, Oak Ridge, Tennessee, 37831-6123, is managed by UT, Battelle, LLC for the Department of Energy under Contract No. DE-AC05-0096OR22725.

Figure Captions:

Figure 1: Mechanism of operation of the Mode Synthesizing Atomic Force Microscope (MSAFM). The dynamics of the cantilever is monitored using an optical readout system (laser). The signal is detected by the lockin amplifier using the difference frequency as reference. The images emerging from MSAFM reveal the presence of nanoparticles below the cell surface.

Figure 2: Protocol for the mice exposure to SWCNHs or silica nanospheres. Each mouse was exposed to 30 μg of SWCNH. Control and SWCNH-exposed mice were sacrificed 24 hours and 7 days post-exposure. Mouse pharyngeal aspiration was used for carbon nanohorn administration. Mice were sacrificed by isoflurane overdose in a bell jar, and BAL was performed according to standard protocols. For light microscopy analysis, cytospin slides were stained with a Hema3 kit (Fisher Scientific). For AFM analysis, cells were centrifuged onto freshly cleaved mica using a cytospin and fixed with methanol. In

addition, peripheral blood was collected using heparinized capillaries from the abdominal aorta. Blood samples were diluted in PBS, centrifuged onto freshly cleaved mica using a cytospin, and fixed with methanol. The samples were characterized using atomic force microscopy (AFM), mode synthesizing force microscopy (MSAFM) and micro-Raman spectroscopy.

Figure 3: Presence of SWCNHs inside the cells obtained from mice lungs. Alveolar macrophages from mice exposed to vehicle control (a-d) and SWCNH after 7 days (e-h). Representative optical (a,e), AFM topography (b,c,f,g), and MSAFM phase (d,h) images from control and treated mice. White dots in (h) (some indicated by the green arrows) correspond to SWCNH.

Figure 4: Images of buried silica nanoparticles in macrophage at different spatial resolution (15 μm, 8 μm and 4 μm scans). (Left) AFM images. (Right) MSAFM phase images obtained by locking on the difference mode Δf. f_c = 4.248 MHz, a_c = 5.4 Vpp, f_s = 3.95 MHz, a_s = 2.2 Vpp.

Figure 5: Chemical signatures of SWCNH in the macrophages using Raman micro-spectroscopy. Raman spectrum of the solution of SWCNH used for the aspiration (a) and of the exposed and non-exposed macrophages (b). The measurements presented were acquired on the macrophages.

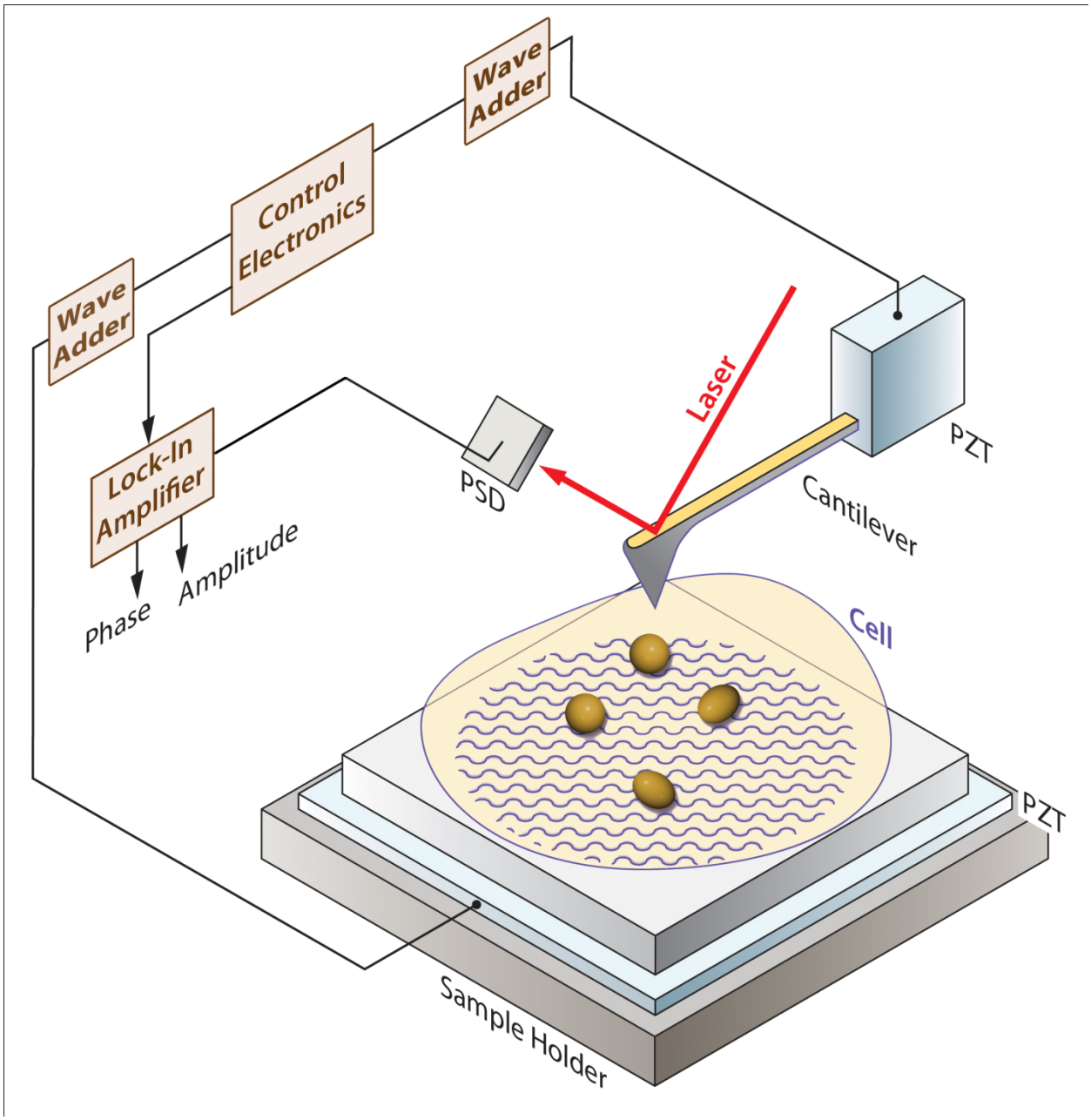

Figure 1: Mechanisms of operation of the Mode Synthesizing Atomic Force Microscope (MSAFM). The dynamics of the cantilever is monitored using an optical readout system (laser). The signal is analyzed in the lockin amplifier using the difference frequency as reference. The images emerging from MSAFM reveal the presence of nanoparticles below the cell surface.

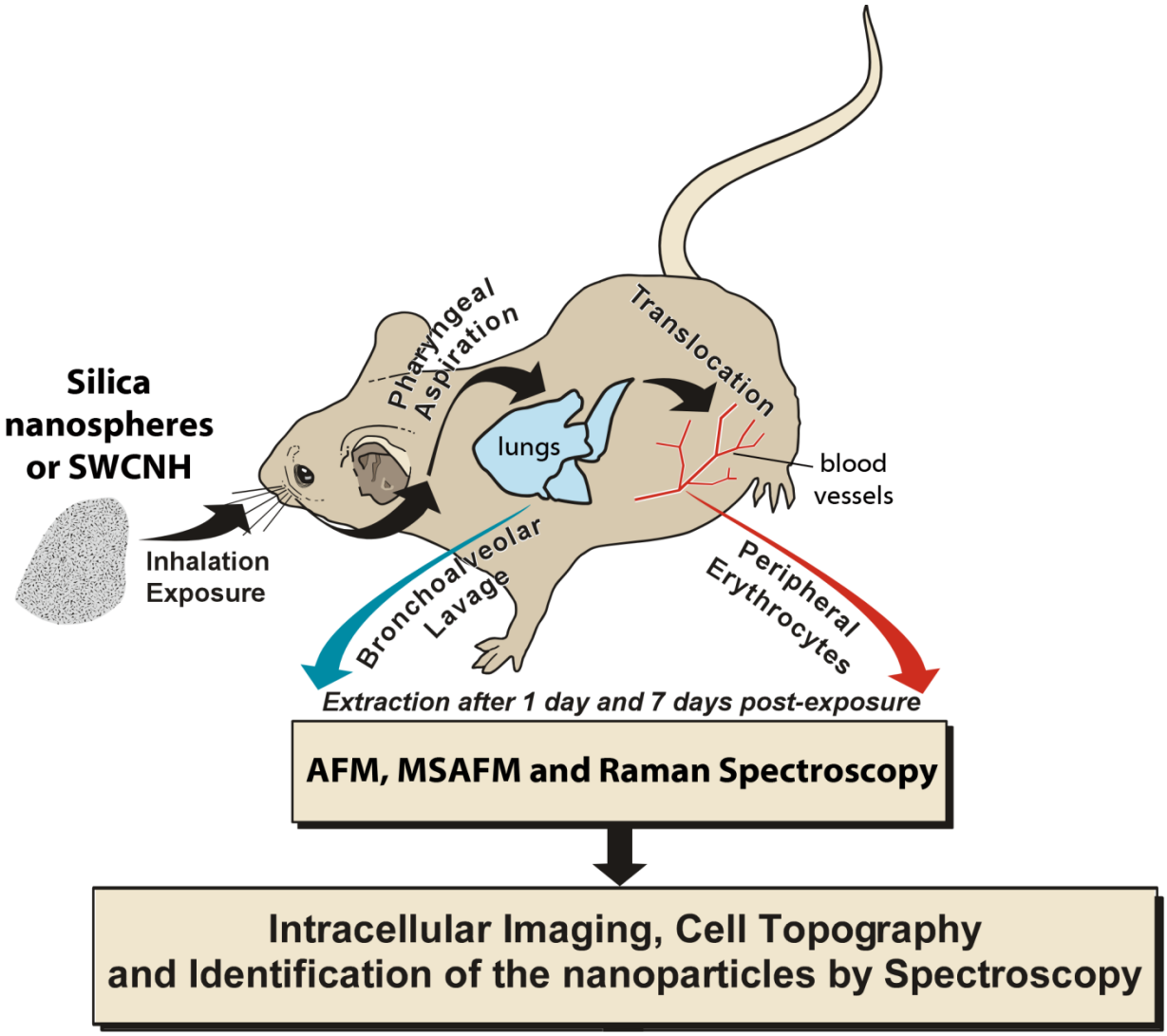

Figure 2: Protocol for the mice exposure to SWCNHs or silica nanospheres. Each mouse was exposed to 30μg of SWCNH. Control and SWCNH-exposed mice were sacrificed 24 hours and 7 days post-exposure. Mouse pharyngeal aspiration was used for carbon nanohorn administration. Mice were sacrificed by isoflurane overdose in a bell jar, and BAL was performed according to standard protocols.For light microscopy analysis, cytospin slides were stained with a Hema3 kit (Fisher Scientific). For AFM analysis, cells were centrifuged onto freshly cleaved mica using a cytospin and fixed with methanol. In addition, peripheral blood was collected using heparinized capillaries from the abdominal aorta. Blood samples were diluted in PBS, centrifuged onto freshly cleaved mica using a cytospin, and fixed with methanol. The samples were characterized using atomic force microscopy (AFM), mode synthesizing force microscopy (MSAFM) and micro-Raman spectroscopy.

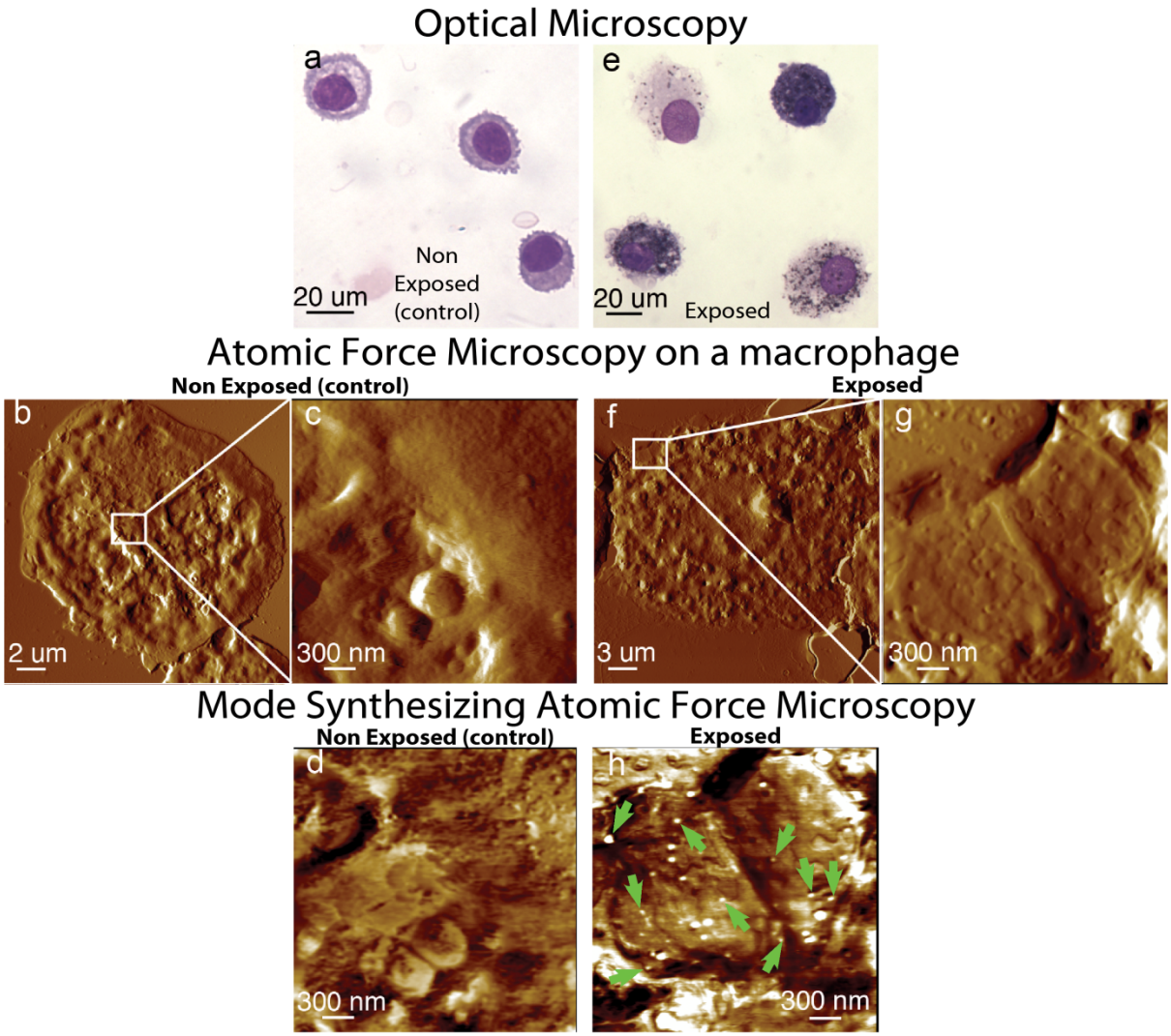

Figure 3: Presence of SWCNHs inside the cells obtained from mice lungs. Alveolar macrophages from vehicle control (a-d) and mice exposed to SWCNH after 7 days (e-h). Representative optical (a,e), AFM topography (b,c,f,g), and MSAFM phase (d,h) images from control and treated mice. White dots in (h) (some indicated by the green arrows) correspond to SWCNH.

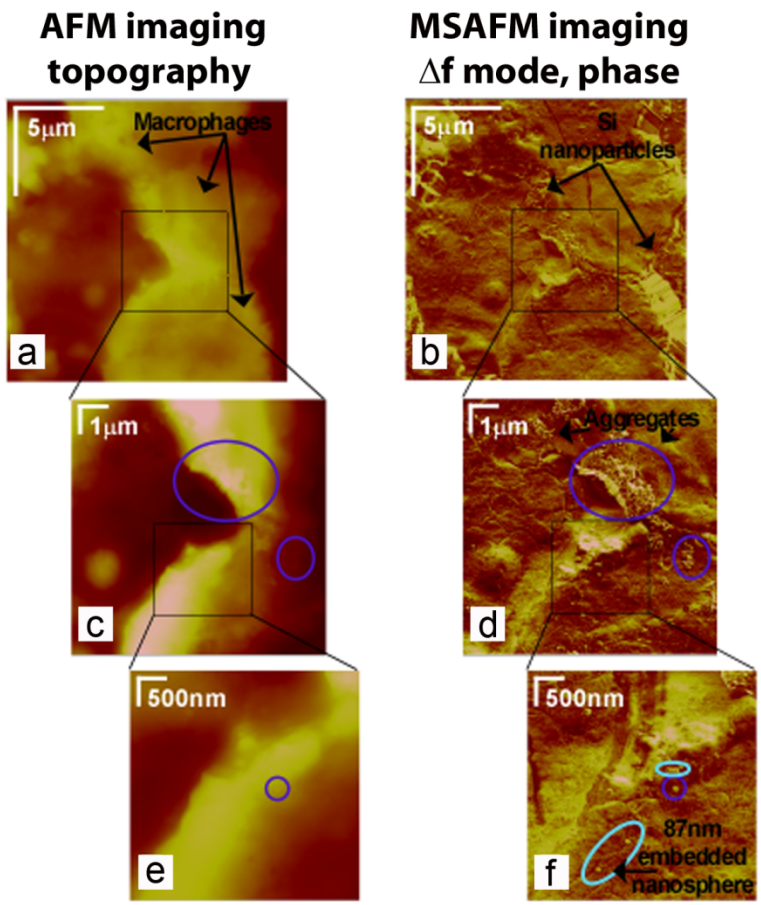

Figure 4: Images of buried silica nanoparticles in macrophage at different spatial resolution (15μm, 8μm and 4μm scans). (Left) AFM images. (Right) MSAFM phase images obtained by lockin on the difference mode Δf. f_c = 4.248 MHz, a_c = 5.4 Vpp, f_s = 3.95 MHz, a_s = 2.2 Vpp.

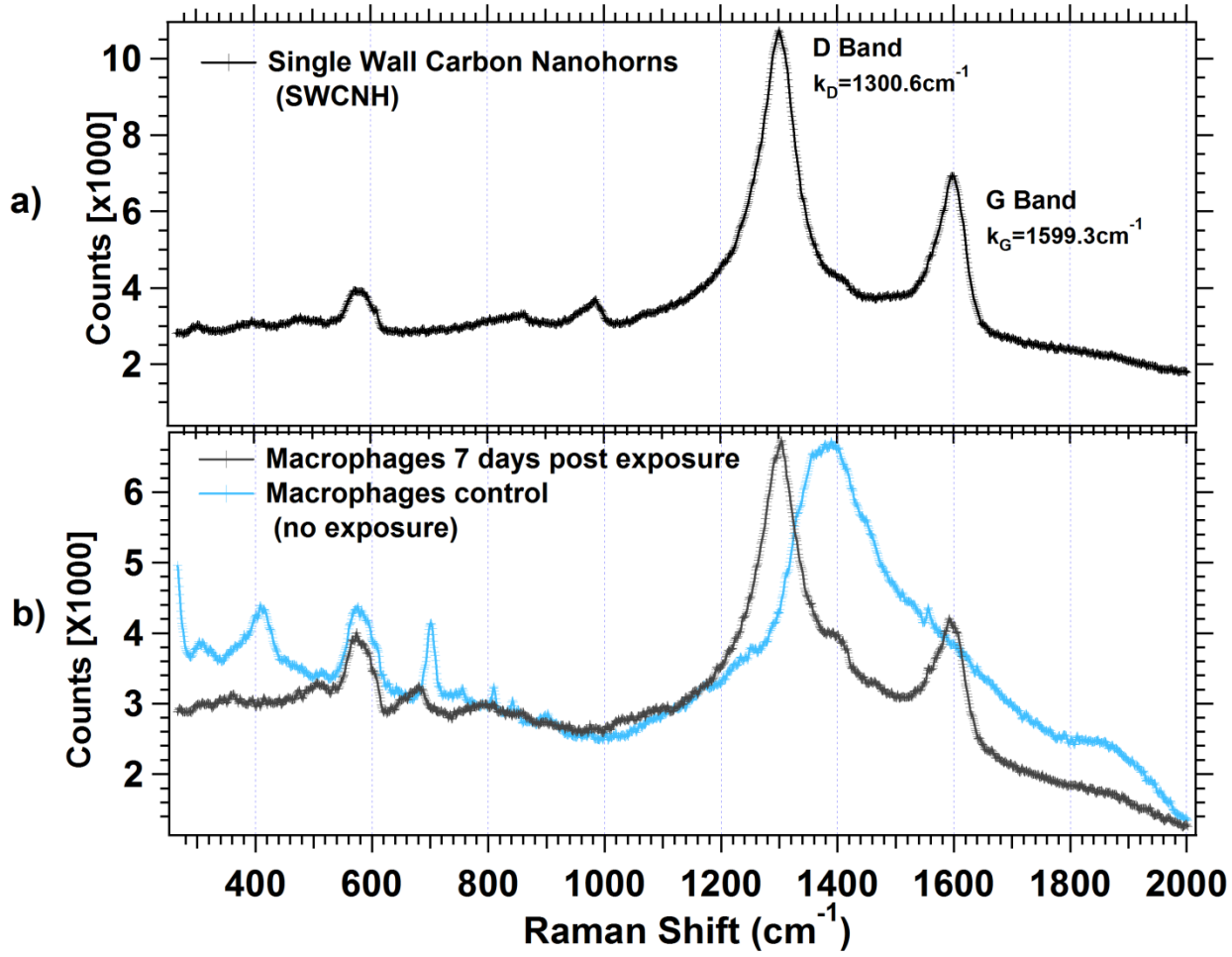

Figure 5: Chemical signatures of SWCNH in the macrophages using Raman micro-spectroscopy. Raman spectrum the solution of SWCNH used for the aspiration (a) and of the exposed and non-exposed macrophages (b). The measurements presented were acquired on a the macrophages.